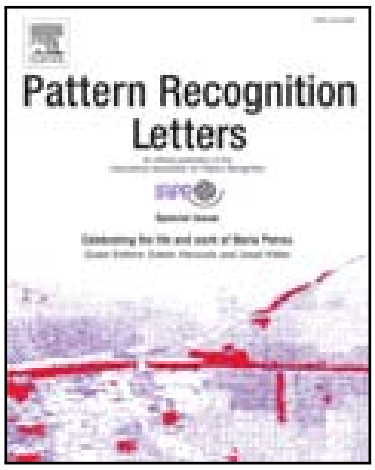

Active Deep neural Network Features Selection for Segmentation and Recognition of Brain Tumors using MRI Images

Muhmmad Irfan Sharif , Jian Ping Li , Muhammad Attique Khan , Muhammad Asim Saleem

PII: S0167-8655(19)30341-1
DOI: https://doi.org/10.1016/j.patrec.2019.11.019
Reference: PATREC 7703

To appear in: *Pattern Recognition Letters*

Received date: 23 September 2019
Revised date: 10 November 2019
Accepted date: 14 November 2019

Please cite this article as: Muhmmad Irfan Sharif , Jian Ping Li , Muhammad Attique Khan , Muhammad Asim Saleem , Active Deep neural Network Features Selection for Segmentation and Recognition of Brain Tumors using MRI Images, *Pattern Recognition Letters* (2019), doi: https://doi.org/10.1016/j.patrec.2019.11.019

Highlights

- A Pixel Increase along Limit (PIaL) based enhancement method is proposed.
- Tumor segmentation is performed through Saliency based deep learning.
- PSO optimization and entropy padding based active features selection.
- A features based extensive comparison is conducted.

Active Deep neural Network Features Selection for Segmentation and Recognition of Brain Tumors using MRI Images

Muhmmad Irfan Sharif[a], Jian Ping Li [a,*], Muhammad Attique Khan[b], Muhammad Asim Saleem[c]
[a],* School of Computer Science and Engineering, University of Electronic Science and Technology of China, Chengdu, China
[b] Department of CS&E, HITEC University, Taxila, Pakistan
[c] School of Information and Software Engineering, University of Electronic Science and Technology of China, Chengdu, China

ABSTRACT

Glioma is a kind of brain tumor that can arise at a distinct location along with dissimilar appearance and size. The high-grade glioma (HGG) is a serious kind of cancer when compare to low-graded glioma (LGG). The manual diagnosis process of these tumors is tiring and time consuming. Therefore, in clinical practices, MRI is useful to assess gliomas as it provides essential information of tumor regions. In this manuscript, an active deep learning-based feature selection approach is suggested to segment and recognize brain tumors. Contrast enhancement is made in the primary step and supplied to SbDL for saliency map construction, which later converts into binarized form by applying simple thresholding. In the classification phase, the Inception V3 pre-trained CNN model is employed for deep feature extraction. These features are simply concatenated along with dominant rotated LBP (DRLBP) for better texture analysis. Later, the concatenated vector is optimized through particle swarm optimization (PSO), so as to classify using softmax classifier. The experiments are conducted in two phases. At first, the segmentation approach SbDL is validated on BRATS2017 and BRATS2018 datasets. The achieved dice score for the BRAST2017 dataset is 83.73% for core tumor, 93.7% for the whole tumor and 79.94% for enhanced tumor. For BRATS2018 dataset, dice score obtained is 88.34% (core), 91.2% (whole) and 81.84% (enhanced). At the second, the classification strategy is applied on BRATS2013, 2014, 2017 and 2018 with an average accuracy of more than 92%. The overall results show that the presented method outperforms for both segmentation and classification of brain tumors.

Keywords- Brain tumor, contrast improvement, deep saliency method, features extraction, optimization, recognition

∗ Corresponding author. Tel.: +0-000-000-0000; fax: +0-000-000-0000; e-mail: jpli2222@uestc.edu.cn

1. Introduction

Gliomas are considered as an alarming and increasing brain tumors which seriously affect human mortality rate [1, 2]. These tumors are characterized into two core types – Low Grade Gliomas (LGG) and High Grade Gliomas (HGG). LGG tumors belong to both benign and malignant classes and its growth rate is very slow in brain cells. Hence, affected patient can survive for several years. On the other side, HGG tumors belong to only malignant class and its growth rate is high in brain cells. Therefore, the anticipatory human life is not more than 2 years [3]. Overall assessment reveals that patients affected with LGG and HGG cannot survive for more than 14 months [4, 5]. The manual diagnosis process of these tumors is tiring and time consuming. As a result, in clinical practices, MRI is useful to assess gliomas as it provides vital information of tumor regions. MRI gives soft tissues contrast when compared to CT and PET images. In MRI, the tumor is categorized into four types. These are T1 weighted (T1W), T1 contrast enhanced (T1CE), T2 weighted (T2W) and Flair, as shown in Figure 1. From all these, Flair scans are the best for separation of edema and CSF regions [6].

There are several semi-automated systems that introduced in literature but in MRI images certain serious challenges are found which affect automated diagnosis process [7]. These challenges are low contrast of MRI scans and change in intensity values. To counter these issues, the computer vision introduced the fully automated systems which composed of four steps that are structure, contrast improvement, noise removal, and segmentation of tumor by using well known techniques including

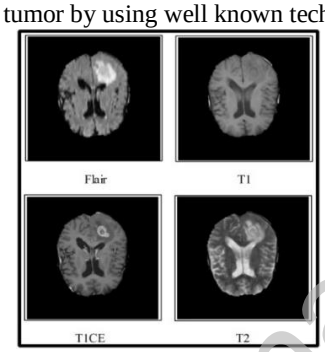

Figure 1: Sample images of brain modalities

clustering, thresholding [8, 9], features extraction (i.e. HOG, LBP, GLCM, geometric and few more) and classification (SVM, KNN, decision trees, etc.) [10-12]. These methods performed better for a limited number of data but when input data increases, the accuracy is degraded considering these methods [13, 14]. To handle these problems, CNN based architectures[15] are introduced which compute automated deep features from original images that are later classified using the softmax classifier [16, 17]. Several CNN methods are presented in the literature for tumor segmentation along with its classification [5, 18].

Most of the existing deep learning models for segmentation and classification are patch based in which one patch of an image is selected for input to the network. The major problem of patch based models includes the loss of core information from an image and also time consuming for training. In general, CNN architecture consists of a hierarchy of many layers. These layers can be convolutional layers, ReLu layers, batch normalization layers, pooling layers, fully connected layers and a softmax classification layer for output. Through these layers, features are calculated directly from complex structure images. A few well known pre-trained CNN models are publicly available namely VGG, Alexnet, GoogleNet, ResNet, Inception and few more [18].

Keeping the aforementioned limitations in mind, the challenge is to detect and recognize multiple modalities as presented in Figure 1. Therefore, texture analysis of these modalities is essential to combine with deep features. But sometimes, all extracted combined features are not essential for accurate classification. recognition accuracy of tumor modalities. The selection of most discriminant features not only reduces the number of predictors but also minimizes overall system execution time. In this work, BRATS series (2013, 2015, 2017, and 2018) is utilized for validation of the proposed system. Our major contributions in this work are:

- Pixel Increase along Limit (PIaL) is showcased to expand the visual quality of the image affected with tumor.
- To construct saliency map with deep and texture features based on distance points for segmentation, a novel SbDL method is suggested.
- An optimization approach is employed using PSO to determine discriminative features from saliency map.
- Finally, based on optimal feature set, classification of brain modalities is conducted.

1. Related Work

In literature, several automated procedures are showcased in the domain of medical imaging for the diagnosis of medical infections such as brain tumor lung cancer [19], skin cancer [20, 21] and more [22, 23]. From all of these, many techniques are presented for an early detection and classification of brain tumor. Subhasis et al. [24] highlight a deep rediomics model for brain tumor detection and classification. They trained the presented model from scratch. After training, transfer learning based fine tuning is performed. Transfer learning is done on two existing deep models that are VGG and ResNet. The LOPO based validation is performed on selected datasets including multi-planar volumetric and achieved an accuracy rate of 95% for both LGG and HGG samples. Ratna et al. [25] presented a search based deep model name HCS-DBN for classification of brain tumors. They used BRATS images for validation. The image is segmented at an initial stage by using a hybrid active contour approach and its features are extracted through HCS-DBN. These features are provided to a classifier and obtained an accuracy level of 94.5%. Amin et al. [26] defined a classical features based method for brain tumor classification. They initially focused on the normalization of original MRI scans and improved them through Weiner filter. Then they performed segmentation through potential field clustering algorithm. In the last step, LBP and Gabor features are computed from the segmented images and fused for final classification. They used BRATS2013 and BRATS2015 datasets for validation and acquired an accuracy of 93% and 97% respectively.

Ahmed et al. [27] suggested a features selection approach for brain tumor classification. They applied two evolutionary algorithms including simulated annealing and genetic algorithm (SA-GA) for selection of optimal features. Two datasets Harvard and Private are used that help to attain accuracy of more than 90%. Surbhi et al. [28] suggested an automated segmented system for brain tumors. They implemented adaptive PSO algorithm along with OTSU method for the segmentation of tumors in MRI. Later, CNN features are extracted and provided to a neural network (NN). Their presented method reflects an accuracy level of 98% with low error rate. Salma et al. [3] suggested a fully automated model for the segmentation of 3D tumor images. Four SegNet models are trained and their information is fused through post processing. The maximum intensity information of original images is encoded to deep features for better representation. Finally, decision tree is used as a classifier for the classification of extracted features. Experimentation is done on BRATS2017 to obtain average F1 Score as 0.80. Kamnitsas et al. [29] presented an 11-layers deep architecture for segmenting the brain tumors in 3D medical images. In the presented method, patches wise training is performed to capture both regional and contextual knowledge of the tumor region. This presented method is evaluated on BRATS2015 and ISLES 2015 datasets and gives better efficiency performance.

An automated method for brain modalities detection and classification is proposed in this research using active deep learning-based features selection. The proposed system is composed of two core architectures that are tumor detection and brain modalities classification. In tumor detection, SbDL segmentation approach is presented, which is further validated on BRATS2017 and BRATS2018 datasets. In modalities classification, pre-trained deep model Inception V3 is fine-tuned and discriminative features are acquired using PSO algorithm. After that, the such features are predicted through softmax classifier. The classification method is evaluated on four datasets named as BRATS2013, BRAST2015, BRATS2017 and BRATS2018. Figure 2 depicts the proposed block diagram.

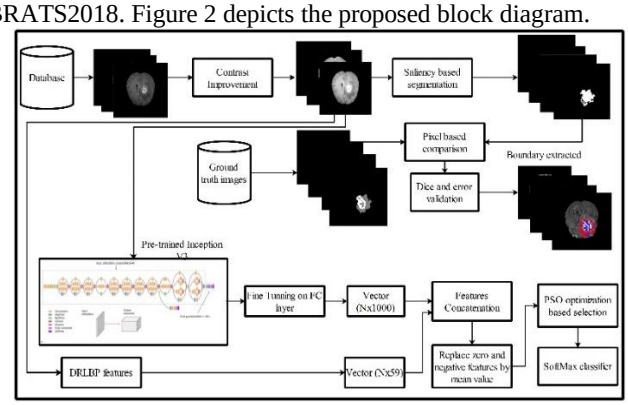

Figure 2: Proposed model of tumor detection and active deep features selection for brain modalities classification.

2.1. Data Contrast Stretching

Contrast improvement is a first and key step of any image processing method. This step reflects pixel intensity difference among the infected and healthy regions. The objective is to clear the visibility of Region of Interest (ROI), which is helpful for accurate tumor segmentation and good features extraction at later stages. Therefore, we adopt contrast stretching to adjust/increase the pixel intensity of the tumor region as per desired range. For this purpose, a simple but an effective approach for contrast stretching named as Pixel Increase along Limit (PIaL) is proposed, which increases the brightness of the infected regions. The proposed PIaL approach improves the pixel intensity value based on sum ($\sum$) parameter α. For doing this, three step model is followed that are: (1) clusters initialization and selection; (2) addition of pixel values through a sum function and; (3) CPD based obtained final resultant image.

As input data is represented by $\Delta \in R$ and each image of Δ is denoted by $\phi(i,j)$, three clusters $C1, C2$ and $C3$ are computed using Equation (1). Equation (1) is defined to divide each image into similar pixels of their range.

$$\begin{cases} C1 \rightarrow C1 \leq \phi(i,j) \leq 100 \\ C2 \rightarrow 101 \leq \phi(i,j) \leq 170 \\ C3 \rightarrow 171 \leq \phi(i,j) \leq 255 \end{cases} \quad (1)$$

From these three clusters, $C3$ is selected for increasing pixel intensity value with the addition of α where $\alpha = 10$. If the range of each pixel intensity value is exceeded 255 after addition of α, then next pixel is considered and current is left as it is. This process is continued till all pixels of $C3$ are processed. Mathematically, the three clusters $C1, C2$, and $C3$ of range $1-100$, $101-170$ and $171-255$ respectively are defined in Equation (2). Each pixel of entire cluster is denoted by c_i, so

$$I_c(i) = \begin{cases} \sum(\alpha)\ if\ C3(i) \leq \beta \\ 0 \quad Otherwise \end{cases} \quad (2)$$

Where, $\beta = 245$. Further, to enhance the tumor contrast, limit expression is applied as in Equations (3) and (4).

$$\lim_{i=0} I_c(i) \frac{1}{K} \sum_{k=0}^{K-1} P_k \quad (3)$$

$$\lim_{i=0} I_c(i) = P_{max} \quad (4)$$

Where, i denotes the clip limit and P_k is a normalized histogram of $C3$. To end this, cumulative probability distribution is enhanced image that can be obtained using Equations (5) -to- (6).

$$H_c = \sum_{c=0}^{K} I_c \quad (5)$$

$$\phi_k(en) = (K-1)H_c \quad (6)$$

Hence, the resultant enhanced image $\phi_k(en)$ is stored into a new database and employed for tumor segmentation. The sample visualizations of this proposed approach are depicted in Figure 3.

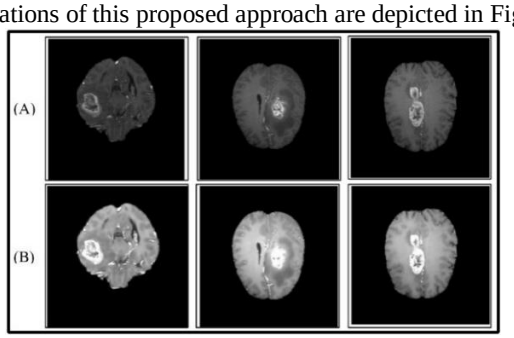

Figure 3: Propose PIaL based contrast improvement results. (A) Original images. (B) PIaL based contrast enhancement.

2.2. Tumor Segmentation

Recently, saliency based segmentation is gaining much interest for diagnosis of infections [10, 30]. In medical image processing, a numerous automated saliency based techniques are introduced which segment infected regions in given images. Nevertheless, due to challenges in medical data, few problems including low contrast lesions, change of tumor shape, change in texture exist which degrades the segmentation performance. To tackle these problems, a new SbDL approach is presented in this research which follows two phase hierarchy.

In the first phase, texture information of an image is extracted using SFTA and LBP features extraction. These feature extraction methods gives low level representation of an object. In the second phase, Alexnet deep CNN pre-trained model is utilized for high level image representation. Later, both low level and high level information is combined through squared Euclidean distance (SED). An illustration of this process is depicted in Figure 4, which demonstrates SbDL visual results. Mathematically, this process is defined as follows:

Enhanced images database is represented as Δ_E and each enhanced image is denoted by $\phi_e(i,j)$ of dimension $N \times M$ where $N,\ M = 256$. Firstly, SFTA features are extracted using the following mathematical expression, given in Equation (9).

$$\phi_{sfta}(U) = \begin{cases} 1 & if\ \exists(i',j') \in N_8[(i,j)]: \\ & \phi_e(i',j') = 0 \wedge \\ & \phi_e(i,j) = 1 \\ 0 & Otherwise \end{cases} \quad (7)$$

Where, $N_8[(i,j)]$ represents the number of connected pixels initialized as 8 in this work.

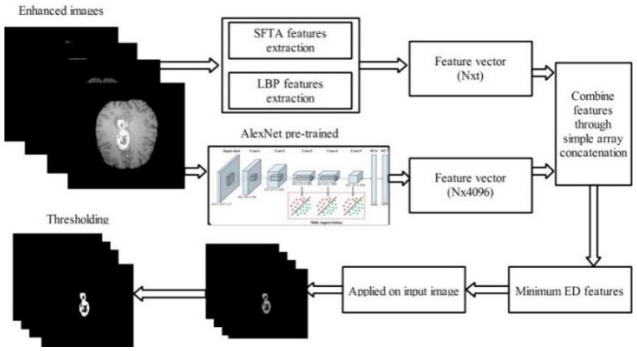

Figure 4: Proposed saliency based tumor segmentation

These features are computed using the boundary complexity of the bright regions (infected areas). This process is performed for all images to obtain a vector of dimension $N \times 21$. After that, LBP features are computed to extract the change of each pixel. Equation (8) is employed for features extraction.

$$\phi_{lbp}(V) = \sum_{v=1}^{8} \lambda(B_i - B_c)2^v \quad (8)$$

$$\lambda(v) = \begin{cases} 1 & if\ v \geq 0 \\ 0 & if\ v < 0 \end{cases} \quad (9)$$

Where, B_i denotes current neighboring pixels and B_c represents central pixel intensity value. The above expression returns a resultant vector of dimension $N \times 59$. Then both vectors are combined by parallel distinct pixel information. Zero padding is performed to make length of both vectors equal. This is done using the Equation (10) given below.

$$\phi_{fv}(U,V) = \begin{cases} \phi_{fv}(W) & for\ \phi(U) \neq \phi(V) \\ Eliminate & for\ \phi(U) = \phi(V) \end{cases} \quad (10)$$

Where, $\phi_{fv}(W)$ denotes combination of distinct features with dissimilar values. However, features with similar values of both vectors are not considered for final low level local fused vector (FV).

In the second phase, deep features are extracted for high level representation of an image. AlexNet deep CNN pre-trained model [31] is fine tuned for this task. In fine tuning process, second last layer is dropped and activation function of stochastic gradient descent (SGD) is applied for features extraction. Mathematically, it is expressed by Equation (11) as:

$$Activation = \theta = \theta - \eta.\varpi_\theta J(\theta; f^{(i)} y^{(i)}; \quad (11)$$

Afterwards, these deep features along with low level representation features are combined by Equation (12) as:

$$\phi_{ff}(X) = \begin{bmatrix} \phi_{fv}(W)_{N\times t} \\ \phi_{df}(W)_{N\times 4096} \end{bmatrix} \quad (12)$$

Then, K-means clustering is performed with K=2. ED is computed for both clusters using Equation (13) and minimum distance features are calculated with Equation (14) for final selection.

$$E(\phi_{ff}(x), k) = \left\|\phi_{ff}(x) - \phi_{ff}(k)\right\|^2 \quad (13)$$

$$\text{argmin}_K \sum_{i=1}^{n} \{\phi_{ff}(x), K(\phi_{ff}, x)\} \quad (14)$$

Through this process, final selected features of each image are mapped on corresponding contrast enhanced image to return a contrast mapped region which is further binarized through Otsu thresholding. The visual results of this process are depicted in Figure 5.

2.3. Tumor Modalities Classification

Object classification is an important step in machine learning applications. In medical research, brain tumor modalities are a challenging classification task. Medical imaging is a very prolific domain from last few years and several techniques are introduced by different researchers [32-34]. A detailed analysis of classical features based techniques in medical imaging, is presented by Acharaya et al. [35]. To follow the conclusion of this work, we implement a deep learning method.

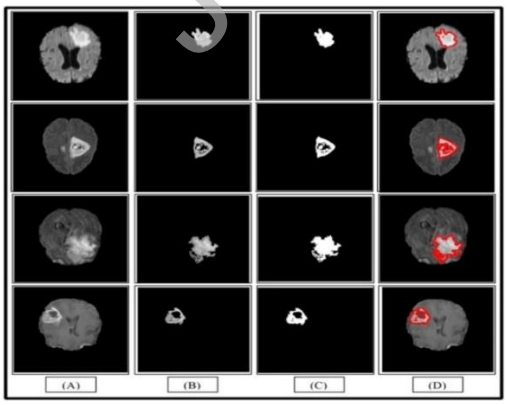

Figure 5: Presented saliency based segmentation (A) Original image. (B) Features mapped. (C) Proposed segmented. (D) Boundary mapped

Referring Figure 1, for classification of these brain modalities, an efficient deep CNN features selection approach is presented in this work which can classify the brain modalities with improved accuracy. A pre-trained CNN deep model Inception V3 is employed for features extraction. This model is popular due to its in table 1.

Table 1: Layers information of Inception V3 Pre-trained CNN

Layer name	Number of layers	Layer name	Number of layers
Image Input Layer	1	Average Pool	9
Scaling Layer	1	Depth Concatenation Layer	15
Batch Normalization Layer	95	FC Layer	1
Convolutional Layer	94	Softmax	1
ReLu	94	Classification	1
MaxPool	4		

Activation function entropy max is applied on FC layer for features extraction. This function returns a vector of dimension $N \times 1000$, which is later fused with dominant rotated LBP features. Later, PSO optimization is performed to select the best optimal features. Entropy padding is employed to equalize the length of each image feature vector. Finally, the finest features are fed to softmax classifier for final classification. This process is presented in Figure 6.

DRLBP features -To compute the texture analysis of brain tumor modalities, weighted Dominant Rotated LBP features are calculated in different rotations. The minimum central pixel difference is considered in this work because tumor modalities are small in size. Mathematically, this is formulated in Equation (15).

$$\xi_D = \text{argmin}_{p\in(0,1,2,\ldots p-1)} |\varphi_p - \varphi_c| \quad (15)$$

Where, p denotes discrete feature values, φ_p denotes the current pixel, and φ_c is central pixel. Hence, final vector is obtained by circular neighborhood direction as in Equation (16) given below.

$$\xi_{drlbp}(r,e) = W \sum_{e=0}^{E-1} \lambda(\varphi_p - \varphi_c) 2^{|e-\xi_D,E|} \quad (16)$$

Where, r denotes the radius of circular neighborhood, W is a weight parameter initialized as 0.1 and updated for each iteration based on mean value,$\xi_{drlbp}()$ denotes DRLBP vector, and e denotes the number of neighbors. The term $2^{|e-\xi_D,E|}$ is always dependent on the central pixel difference (ξ_D) and continuously updated by Eq (15). These features are fast to compute and provide better recognition accuracy in brain modalities classification.

2.3.1. Features Concatenation and Optimization

Finally, both feature vectors (deep CNN and DRLBP) are combines by applying simple array-based concatenation method. The resultant fused FV denoted by ξ_{FV} is of dimension $N \times \boldsymbol{M}$and contains few limitations such as higher computational time and presence of redundant features. To answer this problem, PSO is employed for best solution and entropy value-based padding. Mathematically, it is defined as follows:

As fused vector ξ_{FV} search space is denoted by $\boldsymbol{\Delta}$ and $\boldsymbol{\Delta} \in$ m features, each feature of ξ_{FV} represents a particle located at position $F_i = [f_{i1}, f_{i2}, \ldots, f_{i\Delta}]$ along with velocity $v_i = [v_{i1}, v_{i2}, \ldots, v_{i\Delta}]$, where $i = 1,2,3, \ldots, m$. Each feature $f_{i\Delta}$ moves towards its best position (f_{best}) denoted as $f_{best}(i) = f_b(i) = [f_b(i1), f_b(i2), \ldots, f_b(i\Delta)]$ and the best position of entire search space is $f_{gbest}(i) = f_g(i) = [f_g(1), f_g(2), \ldots, f_g(\Delta)]$.

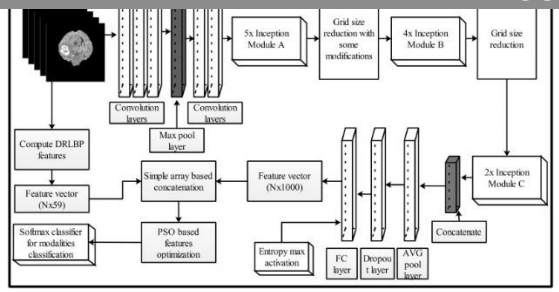

Figure 6: Proposed brain modalities classification process

In search space, each feature changes its position based on velocity value. Mathematically, this process is shown in Equations (17) and (18).

$$v_{id}{}^{t} = w v_{(id)}{}^{(t-1)} + c_1 b_1 (f_b(id)^{(t-1)} - f(id)^{(t-1)}) + c_2 b_2 \left(f_g(d)^{(t-1)} - f(id)^{(t-1)}\right) \quad (17)$$

$$f(id)^{(t)} = f(id)^{(t-1)} + v_{(id)}{}^{(t)} \quad (18)$$

Where, t denotes number of iterations, w is a central radius weight value, c_1, c_2 are constants which drag each feature to $f_b(i)$and $f_g(i)$. The notations $f_b(i)$ and $f_g(i)$ represents the best position and best position entire search space, respectively. The features with maximum velocity are best features and this process is continuous for all features in search space. At last, a $g_{best}(i)$ vector is obtained of dimension $N \times T$, where T denotes the number of best selected features for each image N but vector length issue occurs in this work due to change in number of selected features for N images. To handle this problem, entropy of entire selected vector is computed to perform padding through entropy value. The formula for entropy calculation is expressed in Equation (19).

$$ent = -c_3 \sum_{i=0}^{MAX} S(i) \log(S(i)) \quad (19)$$

Hence, entropy value (ent) is added under selected vector to make features length of all images equal. This vector is denoted by $\xi_{sl}(i)$ and feed to softmax classifier for final classification.

3. Results and Discussion

The proposed method results and comparison with existing techniques in selected datasets are presented in this section. The description of each step is given as follows:

3.1. Dataset description

Propose automated system is validated on four publicly available datasets that are BRATS 2013, BRATS 2015, BRATS 2017 and BRATS 2018 containing HGG and LGG images. In BRATS 2013, a total of 30 HGG/LGG patients' data is available which includes 20 High Graded Gliomas (HGG) and 10 LGG glioma cases. In BRATS 2015, 54 LGG and 220 HGG cases of glioma are provided. BRATS 2017 and 2018 have similar HGG/LGG samples for training. It is bunched with a total of 285 patient's cases including 75 LGG and 210 HGG. The testing glioma cases of BRATS 2017 are 146 of both LGG and HGG whereas BRATS 2018 testing cases are 191, as given in the table 2. Each patient data includes four types of modalities. These are T1, T1CE, T2 and Flair. The resolutions of all images are anisotropic which re-sampled to isotropic.

Table 2: Description about number of selected patients's data for evaluation of proposed system

Dataset	Total Sets	Training Sets	Testing Sets
Brats2013	30	14 HGG 7 LGG	7 HGG 3 LGG
Brats2015	274	154 HGG 38 LGG	66 HGG 16 LGG
Brats2017	431	210 HGG 75 LGG	146 (for both)
Brats2018	476	210 HGG	191 (for both)

3.2. Implementation Minutiae

The presented methodology is executed on MATLAB 2018b using deep learning toolbox Matconvnet [36]. The simulation is executed on Personal Desktop of Corei7 with 16 GB RAM, 128 SSD and a GPU NVIDIA TITAN X. As mentioned above, an entropy max function is employed during the training process with the mini batch size of 64. In addition, a Monte Carlo simulation is performed where the number of iterations is 1000. Three core parameters- error rate, accuracy and overall execution time for all classifiers are evaluated to analyze proposed results.

3.3. Results

In Figure 2 which shows the intended system architecture. It reflects two major contributions. These are tumor segmentation and tumor modalities classification. As both, contributions are independent of each other. Therefore, quantitative and qualitative results of both segmentation and classification are presented separately.

3.3.1. Segmentation results

BRATS 2017- In datasets BRATS 2017 and BRATS 2018 have same training data and ground truths. These are only available for training purposes. Therefore, for the validation of segmentation process using the BRATS 2017 dataset, 100 patients are selected randomly from both HGG and LGG cases. From each case, validation is tested on enhanced tumor, core and whole tumor. Two parameters are calculated that are dice similarity (DS) rate and error rate. The average DS rate for BRATS 2017 dataset is 95.422%, whereas error rate is 4.578%. Moreover, DS rate is also computed for core that is 83.73%, for whole tumor is 93.7%, and for enhanced tumor is 79.94%. DS and error rates of each image are also visually plotted in Figure 7.

For validation of proposed segmentation method on BRATS 2018 dataset, 200 samples are randomly selected from both HGG/LGG patients' cases. The individual DS rate and error rate are computed and demonstrated in Figure 8

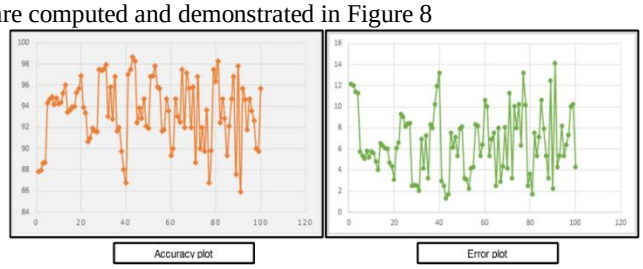

Figure 7: Proposed segmentation performance on BRATS 2017 dataset

The average DS rate is 93.238% whereas error rate is 6.7%. Figure 8 demonstrates that maximum achieved DS rate is 98.4% whereas minimum is 84%. On the other side, maximum error rate is 16% whereas minimum error rate is 1.6%. Moreover, DS rate is also computed for core is 88.34%, for whole tumor is 91.2% and for enhanced tumor is 81.84%. In addition, proposed segmentation results of both selected datasets are also compared with existing techniques. In [37], Wang et al. validated their method on BRATS 2017 dataset and achieved DS rate for enhanced tumor as 78.6%, for whole tumor as 90.5% and for core tumor as 83.8%. Isense et al. [38] achieved DS rate using BRATS 2017 dataset for whole tumor is 85%, for core tumor is 74% and for enhanced tumor is 64%. Presented method achieves DS rate for core tumor is 83.73%, for whole tumor is 93.7% and for enhanced tumor is 79.94%. From results, the presented approach proved its performance better on BRATS 2017 dataset when compared with existing techniques.

Wang et al. [37] also validated their method on BRATS 2018 dataset and achieved DS rate for enhanced tumor as 80.7%, whole tumor as 90.8% and core tumor as 86.9% respectively. Whereas, the proposed method achieved DS rate for core tumor is 88.34%, for whole tumor is 91.2% and for enhanced tumor is

Figure 9, where red line represents suggested method boundary whereas blue line represents ground truth boundary area.

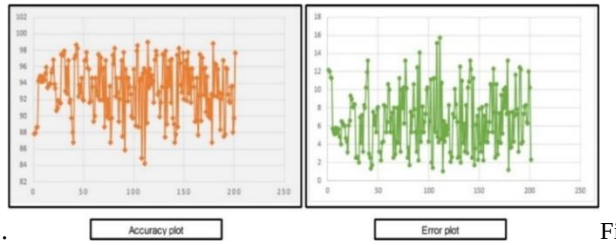

Figure 8: Proposed segmentation performance on BRATS 2018 dataset.

3.3.2. Classification results

The contrast enhanced patients' images are employed for classification. The softmax classifier is selected for predictions. The presented methodology is also assessed with three well known classification algorithms that are MSVM, KNN and ensemble. Four BRATS series datasets including BRATS 2013, 2015, 2017 and 2018 are employed for this process. The performance of each classifier is validated using accuracy, error rate and time parameters. For all datasets, a 70:30 approach is selected for validation along with 10 fold cross validation. Four different types of features combinations are utilized for classification performance- Inception V3 based deep features, DRLBP texture features, fusion of both deep and texture features information and best optimal features.

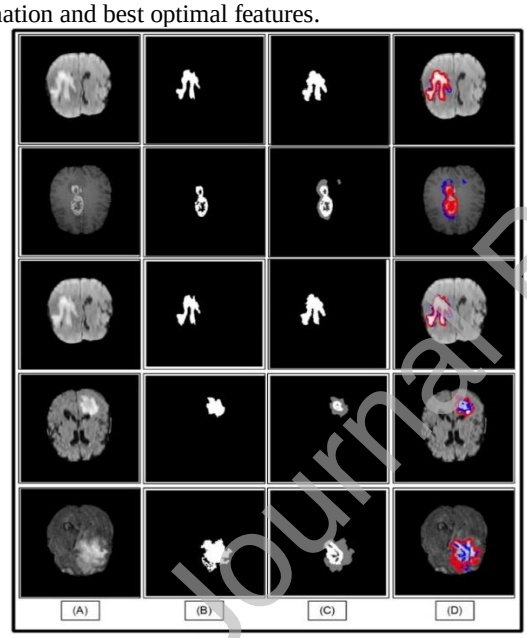

Figure 9: Proposed segmentation results on selected BRATS 2018 dataset. (A) Original image. (B) Proposed segmented. (C) Ground truth image. (D) Detected tumor and ground truth comparison.

BRATS 2013 - The predictions outcomes on BRATS 2013 dataset are given in Table 3. As mentioned above, softmax classifier is utilized in this work and its performance is compared with other classifiers. The softmax classifier achieved an accuracy of 92.8% for CNN features which are computed through Inception V3 pre-trained deep model. The accuracy for texture features is 90.4% which is improved after fusion of both deep and texture features and reached up to 94.7%. In the last, best features are selected and obtained an accuracy of 98.7% along with error rate of 1.3%. The results show that the selection process outperforms individual and fused features. The performance of softmax classifier in comparison with MSVM, KNN and Ensemble methods is given in Table 3. MSVM attained best performance of 92.7% on selected features, KNN obtained 91.1% and ensemble method reached up to 93.8%. Results clearly show the authenticity of proposed deep selected features. In addition, implementation time of each classifier is also noted, given in Table 3 which demonstrated that softmax classifier execution time is good as compared to others.

BRATS 2015 - The predictions outcomes on BRATS 2015 dataset are given in Table 4 which present that maximum achieved accuracy is 97.8% using softmax classifier in selected features. For each modality, average accuracy is 96% and maximum is 99.25% for Flair. The second best attained accuracy of softmax classifier is 95.4% on fused. The softmax classification performance is also compared with three well known methods- MSVM, KNN and ensemble. These methods showed best accuracy of 93.6%, 92.2% and 94.3% on best selected features. In addition, overall execution time of proposed classification architecture is noted and compared with other classifiers, given in Table 4. From Table 4, it is obvious that proposed system perform better on best selected features using softmax classifier.

Table 3: Proposed classification results on BRATS 2013 dataset. The word **TX** denotes texture features, **Fu** denotes fused features, **Sel** denotes selected features and **Acc** denotes accuracy.

Method	**Features**				**Validation measures**		
	CNN	**TX**	**Fu**	**Sel**	**Error (%)**	**Acc (%)**	**Time (sec)**
Softmax	✓				7.2	92.8	64.86
		✓			9.6	90.4	22.90
			✓		**5.3**	**94.7**	**95.76**
				✓	**1.3**	**98.7**	**34.90**
MSVM	✓				9.1	90.9	81.2
		✓			11.4	88.6	37.49
			✓		8.6	91.4	99.62
				✓	7.3	92.7	41.79
KNN	✓				12.6	87.4	110.90
		✓			15.9	84.1	37.49
			✓		9.7	90.3	142.56
				✓	8.9	91.1	43.90
ESDA	✓				8.6	91.4	87.9
		✓			9.2	90.8	42.6
			✓		7.5	92.5	108.97
				✓	6.2	93.8	34.92

Table 4: Proposed classification results on BRATS 2015 dataset

Method	**Features**				**Validation measures**		
	CNN	**TX**	**Fu**	**Sel**	**Error (%)**	**Acc (%)**	**Time (sec)**
Softmax	✓				5.2	94.8	48.96
		✓			5.9	94.1	19.76
			✓		**4.6**	**95.4**	**79.28**
				✓	**2.2**	**97.8**	**21.90**
MSVM	✓				8.6	91.4	72.92
		✓			12.9	87.1	29.68
			✓		7.8	92.2	86.90
				✓	6.4	93.6	36.44
KNN	✓				11.2	88.8	88.42
		✓			14.9	85.1	29.94
			✓		9.6	91.4	96.61
				✓	7.8	92.2	42.60
ESDA	✓				7.6	92.4	91.44
		✓			10.4	89.6	30.70
			✓		6.5	93.5	107.09
				✓	5.7	94.3	44.59

BRATS 2017 - As illustrated in Table 5, the maximum achieved accuracy is 96.90% along with error rate 3.10% using softmax classifier on best selected features. The second best performance is obtained on fused deep and texture features with an accuracy of 95.20% and error rate as 4.80%. Using softmax classifier, the accuracy on individual features is also computed which is improved after fusion and selection process. Moreover, classification results on three other classifiers are also computed for fair comparison of softmax. The best achieved accuracy is 94.10%, 90.20% and 92.70% for MSVM, KNN and ESDA respectively. Finally, overall classification execution time is calculated, given in Table 5 which show that softmax outperforms.

Table 5: Proposed classification results on BRATS 2017 dataset

Method	**Features**	**Validation measures**

	N				r (%)	(%)	(sec)
Softmax	✓				9.60	90.40	71.90
		✓			10.04	89.96	20.96
			✓		**4.80**	**95.20**	86.90
				✓	**3.10**	**96.90**	**28.54**
MSVM	✓				11.10	88.10	73.04
		✓			13.62	86.38	25.46
			✓		8.60	91.40	**81.30**
				✓	5.90	94.10	37.60
KNN	✓				13.74	86.26	88.94
		✓			13.96	86.04	25.51
			✓		11.42	88.58	94.92
				✓	9.80	90.20	31.62
ESDA	✓				9.21	90.79	83.41
		✓			9.98	90.02	31.90
			✓		8.96	91.04	91.99
				✓	7.30	92.70	41.42

BRATS 2018 - Finally, BRATS 2018 dataset results are presented here. The results are given in Table 6 of BRATS 2018 dataset with maximum achieved performance as 92.5% along with error rate 7.5% on best selected features. The second best attained accuracy using softmax classifier is 89.6% on fused features along with error rate of 10.4%. For fair comparison of softmax classifier accuracy on BRATS 2018 dataset, three classifiers MSVM, KNN and Ensemble are selected. On these classifiers, best obtained accuracy is 89.3%, 89%, and 89.10% correspondingly. Moreover, implementation time of all classifiers is given in Table 6. The overall results and execution time show that presented method perform better using softmax classifier on selected features.

Table 6: Proposed classification results on BRATS 2018 dataset

Method	Features				Validation measures		
	CNN	TX	Fu	Sel	Error (%)	Acc (%)	Time (sec)
Softmax	✓				11.9	88.1	67.96
		✓			13.6	86.4	24.90
			✓		**10.4**	**89.6**	**74.46**
				✓	**7.5**	**92.5**	32.41
MSVM	✓				12.6	87.4	75.99
		✓			15.9	84.1	29.04
			✓		11.4	88.6	81.03
				✓	10.7	89.3	37.62
KNN	✓				14.3	85.7	71.48
		✓			14.9	85.1	36.60
			✓		13.6	86.4	79.96
				✓	11.0	89.0	39.42
ESDA	✓				12.3	87.7	81.92
		✓			14.8	85.2	41.09
			✓		12.0	88.0	91.08
				✓	10.9	89.10	**29.61**

3.4. Discussion

A detailed discussion regarding the effect of execution time, variation in proposed results, and comparison with existing techniques is discussed in this section. The results of the proposed approached are computed on different datasets such as BRATS 13, 15, 17, and 18 using a ratio 70:30, which can be view from Table 2 to Table 6. In these tables, it is shown that the best-achieved accuracy is 98.3%, 97.8%, 96.9%, and 92.5%, respectively on the Softmax classifier. The variant performance of the proposed methodology is noticed when we change the classifiers and the proposed selected vector. Besides, this the classification time is also noted and it is observed that the fusion process increases the computational time as compared to individual vector. After fusion, the computational time is almost double but on the other side, the overall accuracy is improved. To handle the problem of execution time, the proposed selection technique is performed which perform better for both accuracy and system efficiency. Before fusion process, the time selection process to $O(n^2)$. At the end, an assessment with existing approaches is also performed and given in Table 7, which demonstrates that proposed classification accuracy is better when compared to existing methods.

Table 7: Comparison of proposed classification accuracy with recent methods

Method	Dataset	Accuracy (%)
Multi-fractal detrended texture feature based method [39]	BRATS2013	86.7
Marker based segmentation and features selection approach [40]	BRATS 2013	98.5
Hybrid active contour model and deep belief network based approach [25]	BRATS2017	94.5
Proposed	**BRATS2013**	**98.3**
Proposed	**BRATS2015**	**97.8**
Proposed	**BRATS2017**	**96.9**
Proposed	**BRATS2018**	**92.5**

4. Conclusion

Novel brain tumor segmentation and multiple brain modalities classification approach are presented. The proposed technique works in two phases: 1) SbDL method for tumor segmentation and validated through DS rate; 2) fusion of deep learning and DRLBP features, which are later optimized through PSO algorithm. The optimized features are validated through a softmax classifier for the classification of different tumor modalities. From the results, it is concluded that a contrast improvement step helps in the construction of better saliency map which later accurately segments the tumor region. Moreover, it is also summed up that although fusion of DRLBP and CNN features increases in classification accuracy but it improves the classification time as well. In a proposed approach, the best features selection step not only increases the accuracy but also minimizes the classification time. In future, this same system can be implemented on Capsule Net for further improvement in overall accuracy.

Declaration of competing interests

On the behalf of corresponding author, all authors declares that they have no conflict of interest.

5. References

[1] S. Bauer, R. Wiest, L.-P. Nolte, and M. Reyes, "A survey of MRI-based medical image analysis for brain tumor studies," *Physics in Medicine & Biology*, vol. 58, p. R97, 2013.

[2] Q. Li, Z. Gao, Q. Wang, J. Xia, H. Zhang, H. Zhang, *et al.*, "Glioma segmentation with a unified algorithm in multimodal MRI images," *IEEE Access*, vol. 6, pp. 9543-9553, 2018.

[3] S. Alqazzaz, X. Sun, X. Yang, and L. Nokes, "Automated brain tumor segmentation on multi-modal MR image using SegNet," *Computational Visual Media*, pp. 1-11.

[4] E. G. Van Meir, C. G. Hadjipanayis, A. D. Norden, H. K. Shu, P. Y. Wen, and J. J. Olson, "Exciting new advances in neuro-oncology: the avenue to a cure for malignant glioma," *CA: a cancer journal for clinicians*, vol. 60, pp. 166-193, 2010.

[5] J. Amin, M. Sharif, M. Yasmin, and S. L. Fernandes, "Big data analysis for brain tumor detection: Deep convolutional neural networks," *Future Generation Computer Systems*, vol. 87, pp. 290-297, 2018.

[6] J. Juan-Albarracín, E. Fuster-Garcia, J. V. Manjon, M. Robles, F. Aparici, L. Martí-Bonmatí, *et al.*, "Automated glioblastoma segmentation based on a multiparametric structured unsupervised classification," *PLoS One*, vol. 10, p. e0125143, 2015.

[7] M. Sharif, U. Tanvir, E. U. Munir, M. A. Khan, and M. Yasmin, "Brain tumor segmentation and classification by improved binomial thresholding and multi-features selection," *Journal of Ambient Intelligence and Humanized Computing*, pp. 1-20, 2018.

[8] ... Fernandes, "Otsu's multi-thresholding and active contour snake model to segment dermoscopy images," *Journal of Medical Imaging and Health Informatics*, vol. 7, pp. 1837-1840, 2017.

[9] N. Dey, V. Rajinikanth, F. Shi, J. M. R. Tavares, L. Moraru, K. A. Karthik, *et al.*, "Social-Group-Optimization based tumor evaluation tool for clinical brain MRI of Flair/diffusion-weighted modality," *Biocybernetics and Biomedical Engineering*, vol. 39, pp. 843-856, 2019.

[10] M. A. Khan, M. Rashid, M. Sharif, K. Javed, and T. Akram, "Classification of gastrointestinal diseases of stomach from WCE using improved saliency-based method and discriminant features selection," *Multimedia Tools and Applications*, pp. 1-28, 2019.

[11] F. Afza, M. A. Khan, M. Sharif, and A. Rehman, "Microscopic skin laceration segmentation and classification: A framework of statistical normal distribution and optimal feature selection," *Microscopy research and technique*, 2019.

[12] M. A. Khan, T. Akram, M. Sharif, A. Shahzad, K. Aurangzeb, M. Alhussein, *et al.*, "An implementation of normal distribution based segmentation and entropy controlled features selection for skin lesion detection and classification," *BMC cancer*, vol. 18, p. 638, 2018.

[13] S. L. Fernandes, V. P. Gurupur, H. Lin, and R. J. Martis, "A Novel fusion approach for early lung cancer detection using computer aided diagnosis techniques," *Journal of Medical Imaging and Health Informatics*, vol. 7, pp. 1841-1850, 2017.

[14] I. NAZ, N. MUHAMMAD, M. YASMIN, M. SHARIF, J. H. SHAH, and S. L. FERNANDES, "ROBUST DISCRIMINATION OF LEUKOCYTES PROTUBERANT TYPES FOR EARLY DIAGNOSIS OF LEUKEMIA," *Journal of Mechanics in Medicine and Biology*, p. 1950055, 2019.

[15] S. Iqbal, M. U. Ghani, T. Saba, and A. Rehman, "Brain tumor segmentation in multi- spectral MRI using convolutional neural networks (CNN)," *Microscopy research and technique*, vol. 81, pp. 419-427, 2018.

[16] M. Sajjad, S. Khan, K. Muhammad, W. Wu, A. Ullah, and S. W. Baik, "Multi-grade brain tumor classification using deep CNN with extensive data augmentation," *Journal of computational science*, vol. 30, pp. 174-182, 2019.

[17] M. Raza, M. Sharif, M. Yasmin, M. A. Khan, T. Saba, and S. L. Fernandes, "Appearance based pedestrians' gender recognition by employing stacked auto encoders in deep learning," *Future Generation Computer Systems*, vol. 88, pp. 28-39, 2018.

[18] T. Yang, J. Song, and L. Li, "A deep learning model integrating SK-TPCNN and random forests for brain tumor segmentation in MRI," *Biocybernetics and Biomedical Engineering*, 2019.

[19] S. A. Khan, M. Nazir, M. A. Khan, T. Saba, K. Javed, A. Rehman, *et al.*, "Lungs nodule detection framework from computed tomography images using support vector machine," *Microscopy research and technique*, 2019.

[20] T. Saba, M. A. Khan, A. Rehman, and S. L. Marie-Sainte, "Region Extraction and Classification of Skin Cancer: A Heterogeneous framework of Deep CNN Features Fusion and Reduction," *Journal of medical systems*, vol. 43, p. 289, 2019.

[21] M. A. Khan, M. Y. Javed, M. Sharif, T. Saba, and A. Rehman, "Multi-Model Deep Neural Network based Features Extraction and Optimal Selection Approach for Skin Lesion Classification," in *2019 International Conference on Computer and Information Sciences (ICCIS)*, 2019, pp. 1-7.

[22] M. Sharif, M. Attique Khan, M. Rashid, M. Yasmin, F. Afza, and U. J. Tanik, "Deep CNN and geometric features-based gastrointestinal tract diseases detection and classification from wireless capsule endoscopy images," *Journal of Experimental & Theoretical Artificial Intelligence*, pp. 1-23, 2019.

[23] A. Liaqat, M. A. Khan, J. H. Shah, M. Sharif, M. Yasmin, and S. L. Fernandes, "Automated ulcer and bleeding classification from WCE images using multiple features fusion and selection," *Journal of Mechanics in Medicine and Biology*, vol. 18, p. 1850038, 2018.

[24] S. Banerjee, S. Mitra, F. Masulli, and S. Rovetta, "Deep Radiomics for Brain Tumor Detection and Classification from Multi-Sequence MRI," *arXiv preprint arXiv:1903.09240*, 2019.

[25] A. R. Raju, S. Pabboju, and R. R. Rao, "Hybrid active contour model and deep belief network based approach for brain tumor segmentation and classification," *Sensor Review*, 2019.

[26] J. Amin, M. Sharif, M. Raza, T. Saba, and M. A. Anjum, "Brain tumor detection using statistical and machine learning method," *Computer Methods and Programs in Biomedicine*, vol. 177, pp. 69-79, 2019.

[27] A. Kharrat and N. Mahmoud, "Feature selection based on hybrid optimization for magnetic resonance imaging brain tumor classification and segmentation," *Applied Medical Informatics*, vol. 41, pp. 9-23, 2019.

[28] S. Vijh, S. Sharma, and P. Gaurav, "Brain Tumor Segmentation Using OTSU Embedded Adaptive Particle Swarm Optimization ... *Visualization and Knowledge Engineering*, ed: Springer, 2020, pp. 171-194.

[29] K. Kamnitsas, C. Ledig, V. F. Newcombe, J. P. Simpson, A. D. Kane, D. K. Menon, *et al.*, "Efficient multi-scale 3D CNN with fully connected CRF for accurate brain lesion segmentation," *Medical image analysis*, vol. 36, pp. 61-78, 2017.

[30] A. Adeel, M. A. Khan, M. Sharif, F. Azam, T. Umer, and S. Wan, "Diagnosis and Recognition of Grape Leaf Diseases: An automated system based on a Novel Saliency approach and Canonical Correlation Analysis based multiple features fusion," *Sustainable Computing: Informatics and Systems*, 2019.

[31] H.-C. Shin, H. R. Roth, M. Gao, L. Lu, Z. Xu, I. Nogues, *et al.*, "Deep convolutional neural networks for computer-aided detection: CNN architectures, dataset characteristics and transfer learning," *IEEE transactions on medical imaging*, vol. 35, pp. 1285-1298, 2016.

[32] M. Sharif, M. A. Khan, M. Faisal, M. Yasmin, and S. L. Fernandes, "A framework for offline signature verification system: Best features selection approach," *Pattern Recognition Letters*, 2018.

[33] J. Amin, M. Sharif, M. Yasmin, and S. L. Fernandes, "A distinctive approach in brain tumor detection and classification using MRI," *Pattern Recognition Letters*, 2017.

[34] S. L Fernandes and J. G Bala, "A novel decision support for composite sketch matching using fusion of probabilistic neural network and dictionary matching," *Current Medical Imaging Reviews*, vol. 13, pp. 176-184, 2017.

[35] U. R. Acharya, S. L. Fernandes, J. E. WeiKoh, E. J. Ciaccio, M. K. M. Fabell, U. J. Tanik, *et al.*, "Automated Detection of Alzheimer's Disease Using Brain MRI Images–A Study with Various Feature Extraction Techniques," *Journal of Medical Systems*, vol. 43, p. 302, 2019.

[36] A. Vedaldi and K. Lenc, "Matconvnet: Convolutional neural networks for matlab," in *Proceedings of the 23rd ACM international conference on Multimedia*, 2015, pp. 689-692.

[37] G. Wang, W. Li, T. Vercauteren, and S. Ourselin, "Automatic Brain Tumor Segmentation Based on Cascaded Convolutional Neural Networks with Uncertainty Estimation," *Frontiers in Computational Neuroscience*, vol. 13, p. 56, 2019.

[38] F. Isensee, P. Kickingereder, W. Wick, M. Bendszus, and K. H. Maier-Hein, "Brain tumor segmentation and radiomics survival prediction: Contribution to the brats 2017 challenge," in *International MICCAI Brainlesion Workshop*, 2017, pp. 287-297.

[39] S. M. Reza, R. Mays, and K. M. Iftekharuddin, "Multi-fractal detrended texture feature for brain tumor classification," in *Medical Imaging 2015: Computer-Aided Diagnosis*, 2015, p. 941410.

[40] M. A. Khan, I. U. Lali, A. Rehman, M. Ishaq, M. Sharif, T. Saba, *et al.*, "Brain tumor detection and classification: A framework of marker-based watershed algorithm and multilevel priority features selection," *Microscopy research and technique*, vol. 82, pp. 909-922, 2019.